Editors' Suggestion

Experimental Realization of Weyl Exceptional Rings in a Synthetic Three-Dimensional Non-Hermitian Phononic Crystal

Jing-jing Liu,[1] Zheng-wei Li,[1] Ze-Guo Chen,[2] Weiyuan Tang,[2] An Chen,[1] Bin Liang,[1,*] Guancong Ma,[2,†] and Jian-Chun Cheng[1,‡]

[1]*Collaborative Innovation Center of Advanced Microstructures and Key Laboratory of Modern Acoustics, MOE, Institute of Acoustics, Department of Physics, Nanjing University, Nanjing 210093, People's Republic of China*

[2]*Department of Physics, Hong Kong Baptist University, Kowloon Tong, Hong Kong, China*

(Received 19 February 2022; accepted 20 July 2022; published 17 August 2022)

Weyl points—topological monopoles of quantized Berry flux—are predicted to spread to Weyl exceptional rings in the presence of non-Hermiticity. Here, we use a one-dimensional Aubry-Andre-Harper model to construct a Weyl semimetal in a three-dimensional parameter space comprising one reciprocal dimension and two synthetic dimensions. The inclusion of non-Hermiticity in the form of gain and loss produces a synthetic Weyl exceptional ring (SWER). The topology of the SWER is characterized by both its topological charge and non-Hermitian winding numbers. We experimentally observe the SWER and synthetic Fermi arc in a one-dimensional phononic crystal with the non-Hermiticity introduced by active acoustic components. Our findings pave the way for studying the high-dimensional non-Hermitian topological physics in acoustics.

DOI: 10.1103/PhysRevLett.129.084301

Introduction.—Topological phenomena were discovered in condensed matter physics, and soon thereafter extended to photonic and phononic crystals (PCs) [1–4]. One important class of three-dimensional (3D) topological systems is the Weyl semimetal, characterized by the existence of Weyl points (WPs)—isolated twofold degeneracies at the crossings of two bands [5,6]. WPs are topological monopoles of quantized Berry flux. In Hermitian crystalline systems, WPs must emerge in pairs and WPs of opposite charges are connected by a surface state called a Fermi arc. WPs have been observed in photonics [7–11], acoustics [12–16], and various condensed matter systems [17–21]. The physics in the vicinity of a WP can typically be captured by a two-level Weyl Hamiltonian containing all the components of Pauli matrices. Such a mathematical form suggests it is impossible to open a gap via Hermitian perturbations. However, perturbations breaking Hermiticity lead to entirely different scenarios. Non-Hermitian systems support a special kind of spectral "degeneracy" called an exceptional point (EP) [22–26], at which one or more state vector(s) become defective. The presence of non-Hermiticity can transform Hermitian degenerate points, such as a Dirac-like point or WP, into an exceptional ring, which is a continuous closed trajectory of EPs in the reciprocal space [27–30]. In particular, the realization of a Weyl exceptional ring in reciprocal space demands fine control of non-Hermitian parameters in a 3D crystal, which is experimentally challenging and so far only realizable in a helical photonic waveguide array [30]. On the other hand, the recent development in the synthetic dimensions indicates that system parameters can be harnessed as degrees of freedom that map to new system dimensions, opening a convenient route to study higher-dimensional physics using systems with fewer real dimensions [8,10,12,31–34].

This Letter presents an experimental realization of the synthetic Weyl exceptional ring (SWER) in a hybrid synthetic-reciprocal space [35] implemented by a PC with actively controlled loss and gain [36,37]. Our system is based on a 1D Aubry-Andre-Harper model [38,39] with both the hopping and on-site energy terms modulated by cosine functions that enforce two independent synthetic dimensions. When non-Hermiticity is introduced, a SWER spawns from the synthetic WP (SWP). Meanwhile, Fermi arcs composed of 0D topological boundary modes are found connecting the two SWPs or two SWERs with different Hermitian topological charges in the synthetic 3D parameter space. Our findings are verified in acoustic experiments. This Letter paves the way to explore high-dimensional non-Hermitian topological physics with low-dimensional PCs.

Theory and design of system.—We start with the following Aubry-Andre-Harper model Hamiltonian,

$$H(k_x,\xi_y,\xi_z)=\begin{pmatrix}\omega_-(\xi_z)-i\gamma_1 & \kappa(k_x,\xi_y)\\ \kappa^*(k_x,\xi_y) & \omega_+(\xi_z)+i\gamma_2\end{pmatrix}, \quad (1)$$

where $\omega_\pm(\xi_z)=\omega_0\pm b_1\cos\xi_z$, $\kappa(k_x,\xi_y)=\kappa_+(\xi_y)+\kappa_-(\xi_y)e^{-ik_xa}$ with $\kappa_+(\xi_y)=-\kappa_0[1+b_2\cos(\xi_y+\pi)]$ and $\kappa_-(\xi_y)=-\kappa_0(1+b_2\cos\xi_y)$ representing the intracell and intercell coupling parameters and $b_1=50$, $b_2=0.5$,

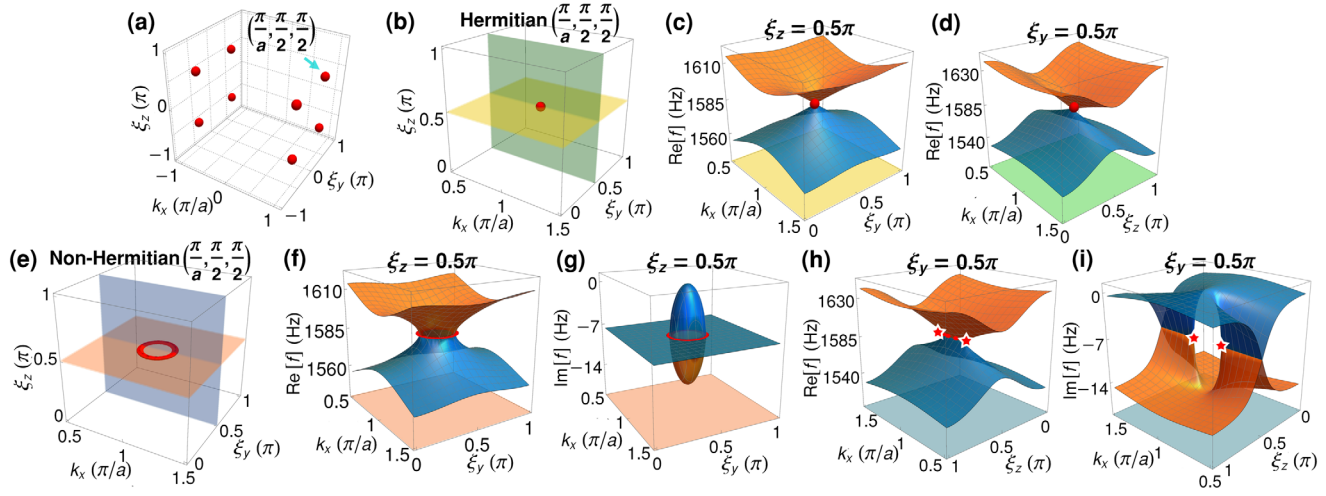

FIG. 1. (a) SWPs in the synthetic-reciprocal space. (b) Schematic of the SWP located at $(\pi/a, \pi/2, \pi/2)$. (c), (d) Band structures in the Hermitian limit in the $k_x\xi_y$ plane at $\xi_z = 0.5\pi$ and $k_x\xi_z$ plane at $\xi_y = 0.5\pi$, respectively. The SWP is marked by the red dot. (e) Schematic of the SWER located at $(\pi/a, \pi/2, \pi/2)$. (f), (g) Real part and imaginary part of the spectrum in the $k_x\xi_y$ plane at $\xi_z = 0.5\pi$ in the non-Hermitian system. A SWER is identified and marked by the red circles. (h), (i) The same system viewed on $k_x\xi_z$ plane for $\xi_y = 0.5\pi$.

a is lattice constant, ω_0 is the premodulation on-site energy, k_x is the Bloch wave number, γ_1, $\gamma_2 \geq 0$. The two imaginary parameters, $-i\gamma_1$ and $i\gamma_2$, respectively, represent loss and gain, which introduce non-Hermiticity. ξ_y and ξ_z are two parameters modulating the hopping and on-site real energy terms. Hence, the eigenstates of Eq. (1) are bundles on a 3D base manifold, in which k_x identifies with $k_x + 2\pi/a$, ξ_y with $\xi_y + 2\pi$, and ξ_z with $\xi_z + 2\pi$. Thus, the base manifold is isomorphic to a 3D torus, which is also isomorphic to a 3D Brillouin zone. Consequently, we can regard ξ_y, ξ_z as two synthetic dimensions, which, together with the reciprocal dimension k_x, make the system described by Eq. (1) effectively a 3D periodic system.

In the Hermitian limit, one has γ_1, $\gamma_2 = 0$, and Eq. (1) gives twofold degenerate points in the synthetic-reciprocal space at $(k_x, \xi_y, \xi_z) = (\pm\pi/a, \pm\pi/2, \pm\pi/2)$, as shown in Fig. 1(a). We analyze the degenerate point at $(\pi/a, \pi/2, \pi/2)$. In its vicinity, the Hamiltonian is, retaining the linear terms,

$$H = \omega_0\sigma_0 + d_x\sigma_x + d_y\sigma_y + d_z\sigma_z, \tag{2}$$

where σ_x, σ_y, σ_z are Pauli matrices and $d_x = -2b_2\kappa_0 \times (\xi_y - 0.5\pi)$, $d_y = -\kappa_0(k_x a - \pi)$, and $d_z = b_1(\xi_z - 0.5\pi)$. Equation (2) takes the form of a Weyl Hamiltonian [17], and the dispersion is linear in all directions.

We characterize the topology of the degenerate point by calculating its Berry charge. To do so, we integrate the Berry curvature over a surface enclosing the point [gray spherical shell in Fig. 2(a)] [28,29,40]:

$$C_m = \frac{1}{2\pi}\int_{\partial\Omega} \vec{A}(\vec{\mu}) \cdot d\vec{S}, \tag{3}$$

where $\vec{A}(\vec{\mu}) = i\langle\nabla_{\vec{\mu}}\psi_m(\vec{\mu})| \times |\nabla_{\vec{\mu}}\psi_m(\vec{\mu})\rangle$ is the local Berry curvature, with ψ_m being the Bloch wave functions of the band and $\mu = k_x, \xi_y, \xi_z$. Our calculations show that $C = \pm 1$, confirming that the twofold degenerate point is a SWP [41]. The charges of the two SWPs at $(\pi/a, \pm\pi/2, \pi/2)$ are opposite, indicating that they form a pair of source and sink for the Berry flux and must be connected by a Fermi arc, as will be shown later.

Next, loss and gain $-i\gamma_1$, $i\gamma_2$ are introduced to the on-site terms of the Hamiltonian, together with a term $-i\gamma_0$ denoting intrinsic background loss. The eigenfrequencies of Eq. (1) take the form

$$\tilde{\omega}_{1,2} = \omega_0 - i\frac{2\gamma_0 + \gamma_1 - \gamma_2}{2} \pm \frac{1}{2}\sqrt{4|\kappa(k_x, \xi_y)|^2 - (\gamma_1 + \gamma_2 - 2ib_1\cos\xi_z)^2}. \tag{4}$$

In doing so, EPs are spawned from the SWP. The SWP morphs into a continuous closed trajectory on the $k_x\xi_y$ plane at $\xi_z = 0.5\pi$, at which the real and imaginary parts of the eigenvalues are identical, as shown in Figs. 1(f) and 1(g). This trajectory is a SWER, with its shape given by

$$(b_2\cos\xi_y)^2 + [1 - (b_2\cos\xi_y)^2]\cos(k_x a) = \left(\frac{\gamma_1 + \gamma_2}{2\sqrt{2}\kappa_0}\right)^2 - 1. \tag{5}$$

Figures 1(h) and 1(i) show the bands on the $k_x\xi_z$ cut plane at $\xi_y = 0.5\pi$, intersecting the SWER at the two points marked by the red stars.

The emergence of the SWER gives rise to richer topological properties, which can be characterized at two different levels. First, similar to the SWP, we can compute the Berry charge of the SWER by integrating the Berry

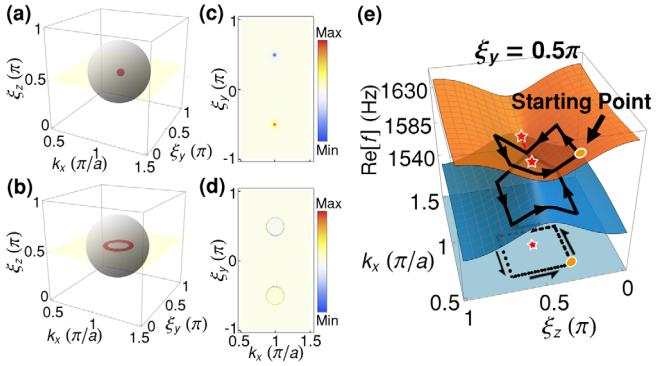

FIG. 2. The gray surfaces enclose (a) the SWP and (b) the SWER for calculating topological charge. And the yellow plane represents the $k_x\xi_y$ plane at $\xi_z = 0.5\pi$. (c),(d) The distribution of the Berry curvature of Hermiticity and non-Hermiticity in the $k_x\xi_y$ plane at $\xi_z = 0.5\pi$, respectively. The color scale indicates the magnitude of the Berry curvature. (e) Schematics of eigenfrequency trajectories for looping around the EP in the $k_x\xi_z$ plane at $\xi_y = 0.5\pi$, which are used to calculate a quantized Berry phase characterizing the EP. The encircled EP is at $(k_x, \xi_z) = (43\pi/50a, \pi/2)$. The bottom is a projection of the loop on the $k_x\xi_z$ plane.

curvature over an enclosing surface, shown in Fig. 2(b). Our results show that $C = \pm 1$, implying that the SWER retains the SWP's topological charge, despite the inclusion of non-Hermiticity. This is further verified by the Berry curvature of two SWPs and SWERs at $(\pi/a, \pm\pi/2, \pi/2)$, as shown in Figs. 2(c) and 2(d). The results also suggest that Fermi arcs survive the inclusion of non-Hermiticity as detailed in the following experimental section. These results agree with related theoretical calculations [28]. Second, the EPs forming the SWER also possess non-Hermitian topology. Unlike Hermitian degeneracies, the topological properties of an EP can be characterized by two methods: eigenvalues and eigenvectors [42,43]. The eigenvalue holonomy around an EP generates a winding number [43–45], given by $\Upsilon = \sum_{j,j'=1}^{2} \epsilon_{j,j'}\nu_{j,j'}$, where j and j' index the states and $j \neq j'$, $\epsilon_{j,j'}$ permutes j and j', $\mu = k_x, \xi_z$. The term

$$\nu_{j,j'} = -\frac{1}{2\pi}\oint \nabla_{\vec{\mu}}\mathrm{Arg}[\omega_j(\vec{\mu}) - \omega_{j'}(\vec{\mu})] \cdot d\vec{\mu} \qquad (6)$$

is called the eigenvalue vorticity [42,46]. By encircling an EP on the SWER as shown in Fig. 2(e), we find $\Upsilon = 1$.

In addition, driving the eigenstates (Bloch wave functions) around the same loop [Fig. 2(e)] produces a non-Hermitian Berry phase given by

$$\theta = \oint i\langle\psi_m(\vec{\mu})|\partial_{\vec{\mu}}\psi_m(\vec{\mu})\rangle \cdot d\vec{\mu}. \qquad (7)$$

Because the evolution of eigenstates is bounded to the non-Hermitian manifold that has two eigenvalue sheets connected at the branch cut, two complete cycles along the encircling path are required for both eigenstates to recover. The total Berry phase after two cycles is $\theta = \pi$ [28]. Hence, the eigenstate winding number is $W = 1/2$.

Experimental results.—The non-Hermitian model is shown in Figs. 3(a) and 3(b). Experimentally, we construct a 1D finite PC with $N = 24$ metal cavities and a circuit part, shown in Fig. 3(c). On-site orbitals are mimicked by the first-order cavity resonance. The pressure profile of the on-site mode is shown at the upper-right panel in Fig. 3(c). Because the eigenfrequency of cavities can be adjusted by the height of cavities, the synthetic dimension ξ_z associated with the on-site modulation can be straightforwardly implemented. The cavities are connected by small tubes to implement the tight-binding hopping $\kappa(k_x, \xi_y)$. The Bloch wave number k_x is naturally realized by the periodicity of the PC. At the same time, by further modulating the tubes' cross-sectional areas, the synthetic dimension ξ_y is realized. The non-Hermiticity in Eq. (1) is introduced as controlled loss and gain. There is no acoustical gain material in nature. To achieve controlled non-Hermiticity, an in-house-designed active unit composed of a loudspeaker, a microphone, and a feedback circuit is installed at the top of each cavity. The amplitude and phase of the emission are precisely controlled according to the signal measured by the microphone. Gain and

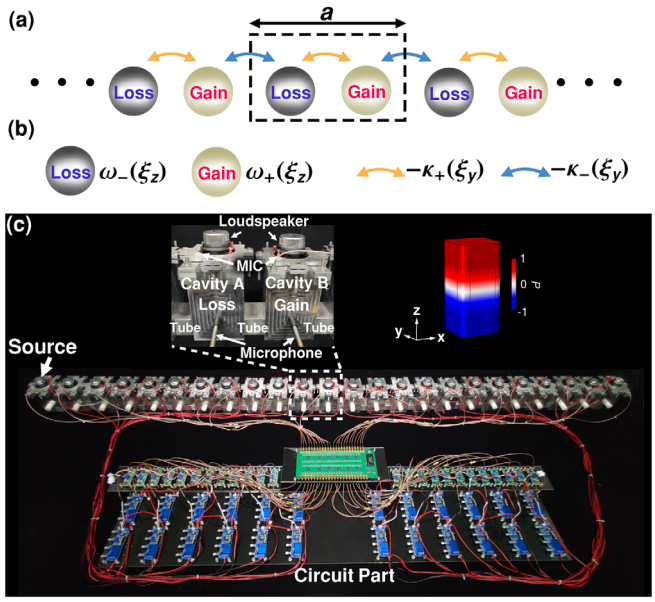

FIG. 3. (a) The 1D non-Hermitian model. The dotted box indicates the unit cell. (b) Loss and gain are introduced to on-site terms and modulated by functions $\omega_\pm(\xi_z)$. The couplings are modulated by functions $-\kappa_\pm(\xi_y)$. (c) The experimental system. The circuits connecting the loudspeakers and microphones at the top of cavities achieve active control of gain and loss in each cavity. The left inset is an enlarged view of a unit cell ($a = 210$ mm). The pressure profile of the cavity's mode is at the right.

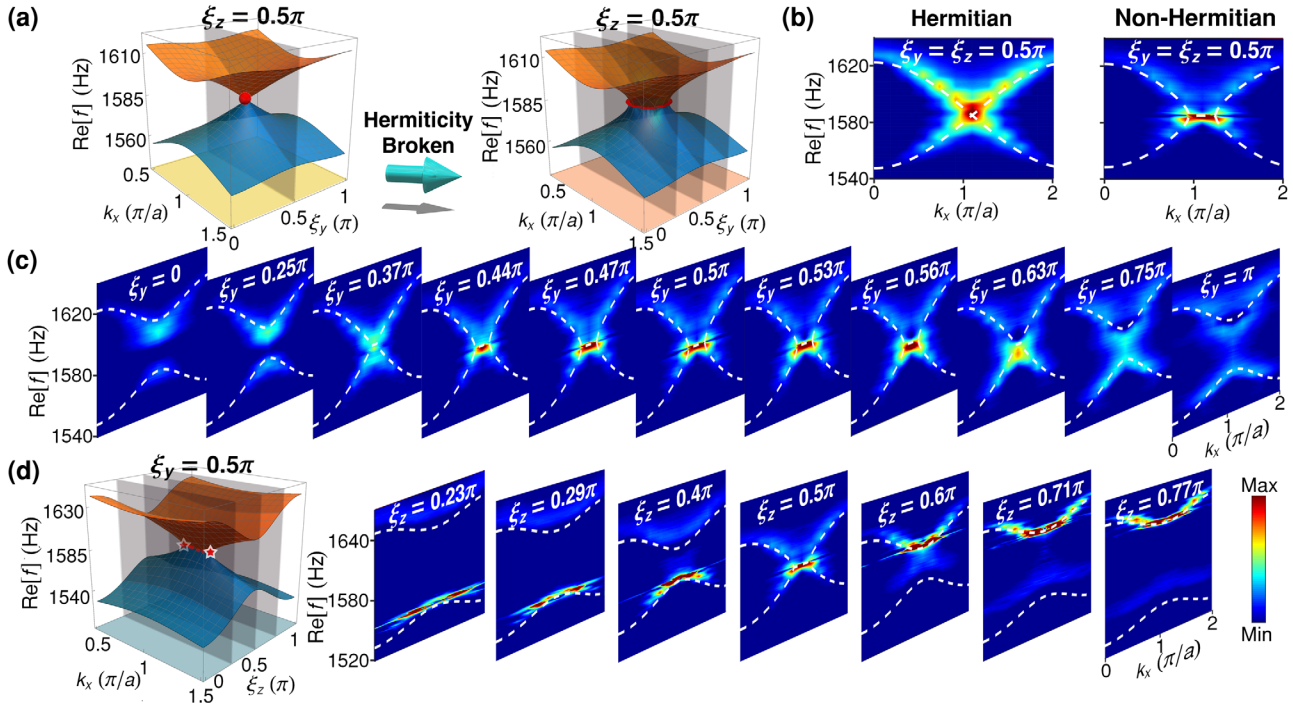

FIG. 4. (a) Schematic of using different planes to cut two band structures. (b) Measured dispersions of the 1D PC. After we add additional loss and gain in the cavities, the point evolves into a nodal line at eigenfrequency ω_0 at $\xi_y = \xi_z = 0.5\pi$. The dashed lines correspond to the numerically calculated band structures of the designed Hamiltonian. (c) For different values of ξ_y at $\xi_z = 0.5\pi$, the images show the evolution of band structures. (d) is similar to (c), but it is for different values of ξ_z at $\xi_y = 0.5\pi$. The SWP becomes a SWER and exists in the $k_x\xi_y$ plane at $\xi_z = 0.5\pi$ in the synthetic momentum space.

loss are introduced when the emission of the loudspeaker is in phase and antiphase with respect to the sound at the top of the cavity, respectively [47]. It should be pointed out that we overcome the self-excitation effect caused by the feedback circuit in gain condition.

We begin with a two-cavity setup to obtain the system parameters of the acoustic system. By using the Green's function and a least-square fitting method [43,48,53], the system parameters are found to be $\omega_0 = 9953.8$ rad/s, $\kappa_0 = 118.7$ rad/s, $\gamma_0 = 30.8$ rad/s, $\gamma_1 = 67.8$ rad/s, and $\gamma_2 = 33.9$ rad/s. Details of the two-cavity experiments and fitting procedures are shown in Ref. [47].

Experimentally, we place an acoustic source at the leftmost cavity of the PC and measure the pressure response spectra in each cavity with a microphone. Fourier transform is then applied to convert the spatial coordinate x to reciprocal coordinate k_x. First, we verify the existence of the SWP. The two synthetic coordinates are set at $\xi_y = \xi_z = 0.5\pi$, as indicated by the gray cut plane at the left of Fig. 4(a). The measured dispersion relation (real part of the frequency) is shown at the left of Fig. 4(b), wherein a continuous band is seen. This band is linear in the vicinity of $k_x = \pi/a$, which agrees well with the theoretical prediction. Next, the non-Hermiticity is introduced by turning on all the active units, which are set to staggeringly generate the gain and loss. In the measured dispersion shown at the right of Fig. 4(b), a flat plateau is developed near $k_x = \pi/a$. This plateau corresponds to the parity-time-broken phase, at which the real parts of the eigenfrequencies are degenerate. The two endpoints of this plateau are two EPs on the SWER. We further obtain the dispersion at 11 different ξ_y with $\xi_z = 0.5\pi$, as shown in Fig. 4(c). The dispersion curves are gapped for $\xi_y < 0.37\pi$ and $\xi_y > 0.63\pi$. The plateau can be clearly identified in $0.44\pi \le \xi_y \le 0.56\pi$. The plateau's width increases until $\xi_y = 0.5\pi$ and then decreases and eventually vanishes at $\xi_y = 0.63\pi$. The endpoints of the plateau clearly delineate a closed loop on the $k_x\xi_y$ plane at $\xi_z = 0.5\pi$, which validates the existence of the SWER. We repeat the measurement with $\xi_y = 0.5\pi$ and then tune ξ_z to 7 different values. In the results plotted in Fig. 4(d), we can identify a gap that closes only at $\xi_z = 0.5\pi$ in the formation of a plateau. From this observation, we conclude that the SWER indeed lies on the $k_x\xi_y$ plane at $\xi_z = 0.5\pi$.

The presence of the SWPs indicates the existence of Fermi arcs that are 2D surface states pinned by a pair of SWPs with opposite topological charges in a finite-sized system. In our system, the Fermi arcs are observed as 0D topological boundary modes localized at the two ends of the real-space PC. Fermi arcs are generally dispersive curves in the reciprocal dimensions. In the Hermitian case, sublattice symmetry protects the Fermi arcs to be

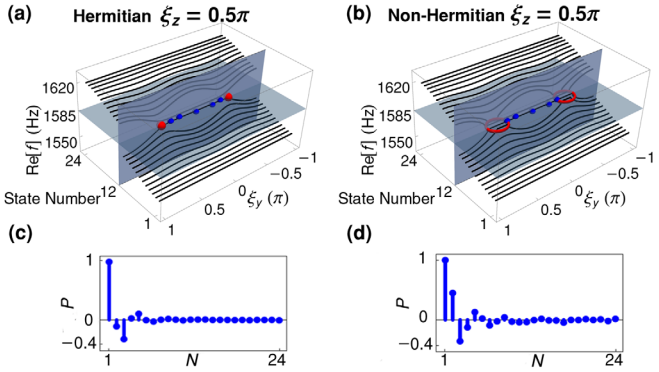

FIG. 5. The real spectra of a 24-site lattice with an open boundary and $\xi_z = 0.5\pi$ of the Hermitian (a) and non-Hermitian case (b). The blue dots are measured results of the Fermi arcs. The measured pressure fields of edge states at $\xi_y = 0$ for Hermitian (c) and non-Hermitian case (d).

near-zero-energy flat bands in $\xi_y \in (-0.5\pi, 0.5\pi)$ at $\xi_z = 0.5\pi$, as shown in Fig. 5(a). In the non-Hermitian case, the finite system obeys anti-pseudo-Hermiticity and parity-time symmetry, such that the real parts of the spectrum are symmetric and the two Fermi arcs are pinned to zero real energy as flat bands that connect the SWERs [Fig. 5(b)] (see Ref. [47] for more details). We have measured the Fermi arcs composed of edge states experimentally for both the Hermitian and non-Hermitian cases at a series of ξ_y, as shown in Figs. 5(a) and 5(b). Slight deviation from zero energy is attributable to experimental errors. Figures 5(c) and 5(d) show the measured edge states at $\xi_y = 0$. It is noteworthy that the flat Fermi arcs, the SWER, and the bulk states therein have identical real eigenfrequencies—an interesting property useful for applications such as wave routing, which we demonstrate in [47].

Conclusion.—We have experimentally realized a SWP and a SWER in a 1D non-Hermitian PC with two synthetic dimensions. Our results show that EP structures appearing in the Bloch bands of non-Hermitian systems can be investigated in hybrid reciprocal-synthetic systems, which are experimentally more convenient and versatile compared to systems with pure spatial periodicity. And the fact that SWERs can merge to realize a topological phase transition dependent only on the strength of the non-Hermiticity allows for a new route to obtaining tunable phononic topological materials. We have also developed an acoustic system with the successful implementation of actively tunable loss and gain, which can serve as a platform for studying more sophisticated non-Hermitian phenomena, such as non-Hermitian skin effects [25,54,55], EP chains [43], and EP links [56].

This work was supported by National Key R&D Program of China (2017YFA0303700), the National Natural Science Foundation of China (11922416, 11634006, 11374157, 81127901, 11704284), Hong Kong Research Grant Council (RFS2223-2S01, 12300419, 12302420, 12301822), a project funded by the Priority Academic Program Development of Jiangsu Higher Education Institutions and High-Performance Computing Center of Collaborative Innovation Center of Advanced Microstructures.

J.-J. L., Z-W. L., and Z.-G. C. contributed equally to this work.

*Corresponding author.
liangbin@nju.edu.cn
†Corresponding author.
phgcma@hkbu.edu.hk
‡Corresponding author.
jccheng@nju.edu.cn

[1] M. Z. Hasan and C. L. Kane, Colloquium: Topological insulators, Rev. Mod. Phys. **82**, 3045 (2010).
[2] X.-L. Qi and S.-C. Zhang, Topological insulators and superconductors, Rev. Mod. Phys. **83**, 1057 (2011).
[3] T. Ozawa, H. M. Price, A. Amo, N. Goldman, M. Hafezi, L. Lu, M. C. Rechtsman, D. Schuster, J. Simon, O. Zilberberg, and I. Carusotto, Topological photonics, Rev. Mod. Phys. **91**, 015006 (2019).
[4] G. Ma, M. Xiao, and C. T. Chan, Topological phases in acoustic and mechanical systems, Nat. Rev. Phys. **1**, 281 (2019).
[5] C. Fang, M. J. Gilbert, X. Dai, and B. A. Bernevig, Multi-Weyl Topological Semimetals Stabilized by Point Group Symmetry, Phys. Rev. Lett. **108**, 266802 (2012).
[6] N. P. Armitage, E. J. Mele, and A. Vishwanath, Weyl and dirac semimetals in three-dimensional solids, Rev. Mod. Phys. **90**, 015001 (2018).
[7] W.-J. Chen, M. Xiao, and C. T. Chan, Photonic crystals possessing multiple Weyl points and the experimental observation of robust surface states, Nat. Commun. **7**, 13038 (2016).
[8] Q. Lin, M. Xiao, L. Yuan, and S. Fan, Photonic Weyl point in a two-dimensional resonator lattice with a synthetic frequency dimension, Nat. Commun. **7**, 13731 (2016).
[9] L. Lu, Z. Wang, D. Ye, L. Ran, L. Fu, J. D. Joannopoulos, and M. Soljačić, Experimental observation of Weyl points, Science **349**, 622 (2015).
[10] Q. Wang, M. Xiao, H. Liu, S. Zhu, and C. T. Chan, Optical Interface States Protected by Synthetic Weyl Points, Phys. Rev. X **7**, 031032 (2017).
[11] B. Yang, Q. Guo, B. Tremain, R. Liu, L. E. Barr, Q. Yan, W. Gao, H. Liu, Y. Xiang, J. Chen *et al.*, Ideal Weyl points and helicoid surface states in artificial photonic crystal structures, Science **359**, 1013 (2018).
[12] X. Fan, C. Qiu, Y. Shen, H. He, M. Xiao, M. Ke, and Z. Liu, Probing Weyl Physics with One-Dimensional Sonic Crystals, Phys. Rev. Lett. **122**, 136802 (2019).
[13] H. He, C. Qiu, L. Ye, X. Cai, X. Fan, M. Ke, F. Zhang, and Z. Liu, Topological negative refraction of surface acoustic waves in a Weyl phononic crystal, Nature (London) **560**, 61 (2018).

[14] F. Li, X. Huang, J. Lu, J. Ma, and Z. Liu, Weyl points and fermi arcs in a chiral phononic crystal, Nat. Phys. **14**, 30 (2018).
[15] L. Lu, L. Fu, J. D. Joannopoulos, and M. Soljačić, Weyl points and line nodes in gyroid photonic crystals, Nat. Photonics **7**, 294 (2013).
[16] M. Xiao, W.-J. Chen, W.-Y. He, and C. T. Chan, Synthetic gauge flux and Weyl points in acoustic systems, Nat. Phys. **11**, 920 (2015).
[17] X. Wan, A. M. Turner, A. Vishwanath, and S. Y. Savrasov, Topological semimetal and fermi-arc surface states in the electronic structure of pyrochlore iridates, Phys. Rev. B **83**, 205101 (2011).
[18] D. Liu, A. Liang, E. Liu, Q. Xu, Y. Li, C. Chen, D. Pei, W. Shi, S. Mo, P. Dudin *et al.*, Magnetic Weyl semimetal phase in a kagomé crystal, Science **365**, 1282 (2019).
[19] B. Q. Lv, H. M. Weng, B. B. Fu, X. P. Wang, H. Miao, J. Ma, P. Richard, X. C. Huang, L. X. Zhao, G. F. Chen, Z. Fang, X. Dai, T. Qian, and H. Ding, Experimental Discovery of Weyl Semimetal TaAs, Phys. Rev. X **5**, 031013 (2015).
[20] S.-Y. Xu, I. Belopolski, N. Alidoust, M. Neupane, G. Bian, C. Zhang, R. Sankar, G. Chang, Z. Yuan, C.-C. Lee *et al.*, Discovery of a Weyl fermion semimetal and topological fermi arcs, Science **349**, 613 (2015).
[21] S.-Y. Xu, I. Belopolski, D. S. Sanchez, C. Zhang, G. Chang, C. Guo, G. Bian, Z. Yuan, H. Lu, T.-R. Chang *et al.*, Experimental discovery of a topological Weyl semimetal state in TaP, Sci. Adv. **1**, e1501092 (2015).
[22] E. J. Bergholtz, J. C. Budich, and F. K. Kunst, Exceptional topology of non-Hermitian systems, Rev. Mod. Phys. **93**, 015005 (2021).
[23] C. M. Bender, S. Boettcher, and P. N. Meisinger, PT-symmetric quantum mechanics, J. Math. Phys. (N.Y.) **40**, 2201 (1999).
[24] C. M. Bender, D. C. Brody, and H. F. Jones, Complex Extension of Quantum Mechanics, Phys. Rev. Lett. **89**, 270401 (2002).
[25] S. Yao and Z. Wang, Edge States and Topological Invariants of Non-Hermitian Systems, Phys. Rev. Lett. **121**, 086803 (2018).
[26] Ş. K. Özdemir, S. Rotter, F. Nori, and L. Yang, Parity–time symmetry and exceptional points in photonics, Nat. Mater. **18**, 783 (2019).
[27] B. Zhen, C. W. Hsu, Y. Igarashi, L. Lu, I. Kaminer, A. Pick, S.-L. Chua, J. D. Joannopoulos, and M. Soljačić, Spawning rings of exceptional points out of Dirac cones, Nature (London) **525**, 354 (2015).
[28] Y. Xu, S.-T. Wang, and L.-M. Duan, Weyl Exceptional Rings in a Three-Dimensional Dissipative Cold Atomic Gas, Phys. Rev. Lett. **118**, 045701 (2017).
[29] A. Cerjan, M. Xiao, L. Yuan, and S. Fan, Effects of non-hermitian perturbations on Weyl hamiltonians with arbitrary topological charges, Phys. Rev. B **97**, 075128 (2018).
[30] A. Cerjan, S. Huang, M. Wang, K. P. Chen, Y. Chong, and M. C. Rechtsman, Experimental realization of a Weyl exceptional ring, Nat. Photonics **13**, 623 (2019).
[31] O. Boada, A. Celi, J. I. Latorre, and M. Lewenstein, Quantum Simulation of an Extra Dimension, Phys. Rev. Lett. **108**, 133001 (2012).
[32] M. Lohse, C. Schweizer, H. M. Price, O. Zilberberg, and I. Bloch, Exploring 4D quantum Hall physics with a 2D topological charge pump, Nature (London) **553**, 55 (2018).
[33] Y. E. Kraus, Y. Lahini, Z. Ringel, M. Verbin, and O. Zilberberg, Topological States and Adiabatic Pumping in Quasicrystals, Phys. Rev. Lett. **109**, 106402 (2012).
[34] T. Ozawa, H. M. Price, N. Goldman, O. Zilberberg, and I. Carusotto, Synthetic dimensions in integrated photonics: From optical isolation to four-dimensional quantum Hall physics, Phys. Rev. A **93**, 043827 (2016).
[35] S. Ganeshan and S. Das Sarma, Constructing a Weyl semimetal by stacking one-dimensional topological phases, Phys. Rev. B **91**, 125438 (2015).
[36] R. Fleury, D. Sounas, and A. Alù, An invisible acoustic sensor based on parity-time symmetry, Nat. Commun. **6**, 5905 (2015).
[37] C. Shi, M. Dubois, Y. Chen, L. Cheng, H. Ramezani, Y. Wang, and X. Zhang, Accessing the exceptional points of parity-time symmetric acoustics, Nat. Commun. **7**, 11110 (2016).
[38] P. G. Harper, Single band motion of conduction electrons in a uniform magnetic field, Proc. Phys. Soc. London Sect. A **68**, 874 (1955).
[39] J. Biddle, D. J. Priour, B. Wang, and S. Das Sarma, Localization in one-dimensional lattices with non-nearest-neighbor hopping: Generalized Anderson and Aubry-André models, Phys. Rev. B **83**, 075105 (2011).
[40] T. Fukui, Y. Hatsugai, and H. Suzuki, Chern numbers in discretized brillouin zone: Efficient method of computing (spin) Hall conductances, J. Phys. Soc. Jpn. **74**, 1674 (2005).
[41] A. A. Soluyanov, D. Gresch, Z. Wang, Q. Wu, M. Troyer, X. Dai, and B. A. Bernevig, Type-II Weyl semimetals, Nature (London) **527**, 495 (2015).
[42] H. Shen, B. Zhen, and L. Fu, Topological Band Theory for Non-Hermitian Hamiltonians, Phys. Rev. Lett. **120**, 146402 (2018).
[43] W. Tang, K. Ding, and G. Ma, Direct Measurement of Topological Properties of an Exceptional Parabola, Phys. Rev. Lett. **127**, 034301 (2021).
[44] K. Kawabata, K. Shiozaki, M. Ueda, and M. Sato, Symmetry and Topology in Non-Hermitian Physics, Phys. Rev. X **9**, 041015 (2019).
[45] Z. Yang, A. P. Schnyder, J. Hu, and C.-K. Chiu, Fermion Doubling Theorems in Two-Dimensional Non-Hermitian Systems for Fermi Points and Exceptional Points, Phys. Rev. Lett. **126**, 086401 (2021).
[46] D. Leykam, K. Y. Bliokh, C. Huang, Y. D. Chong, and F. Nori, Edge Modes, Degeneracies, and Topological Numbers in Non-Hermitian Systems, Phys. Rev. Lett. **118**, 040401 (2017).
[47] See Supplemental Materials at http://link.aps.org/supplemental/10.1103/PhysRevLett.129.084301 for more details in the experimental system, parameter retrieval, and an example of energy-splitting application, which includes Refs. [6,17,36,37,48–52].
[48] K. Ding, G. Ma, M. Xiao, Z. Q. Zhang, and C. T. Chan, Emergence, Coalescence, and Topological Properties of Multiple Exceptional Points and Their Experimental Realization, Phys. Rev. X **6**, 021007 (2016).

[49] M. Sato, K. Hasebe, K. Esaki, and M. Kohmoto, Time-reversal symmetry in non-Hermitian systems, Prog. Theor. Phys. **127**, 937 (2012).

[50] A. Mostafazadeh, Pseudo-Hermiticity versus PT-symmetry III: Equivalence of pseudo-Hermiticity and the presence of antilinear symmetries, J. Math. Phys. (N.Y.) **43**, 3944 (2002).

[51] Z. Xu, R. Zhang, S. Chen, L. Fu, and Y. Zhang, Fate of zero modes in a finite Su-Schrieffer-Heeger model with $\mathcal{PT}$ symmetry, Phys. Rev. A **101**, 013635 (2020).

[52] W. Song, W. Sun, C. Chen, Q. Song, S. Xiao, S. Zhu, and T. Li, Breakup and Recovery of Topological Zero Modes in Finite Non-Hermitian Optical Lattices, Phys. Rev. Lett. **123**, 165701 (2019).

[53] W. Tang, X. Jiang, K. Ding, Y.-X. Xiao, Z.-Q. Zhang, C. T. Chan, and G. Ma, Exceptional nexus with a hybrid topological invariant, Science **370**, 1077 (2020).

[54] D. S. Borgnia, A. J. Kruchkov, and R.-J. Slager, Non-Hermitian Boundary Modes and Topology, Phys. Rev. Lett. **124**, 056802 (2020).

[55] N. Okuma, K. Kawabata, K. Shiozaki, and M. Sato, Topological Origin of Non-Hermitian Skin Effects, Phys. Rev. Lett. **124**, 086801 (2020).

[56] J. Geldmeier, P. Johns, N. J. Greybush, J. Naciri, and J. Fontana, Plasmonic aerosols, Phys. Rev. B **99**, 081112(R) (2019).